IEEE Access
Multidisciplinary : Rapid Review : Open Access Journal

Received November 14, 2018, accepted November 30, 2018, date of publication December 7, 2018, date of current version January 4, 2019.

Digital Object Identifier 10.1109/ACCESS.2018.2885535

Empirical Frequency-Dependent Wall Insertion Loss Model at 3–6 GHz for Future Internet-of-Things Applications

YANG LIU[1,2], (Member, IEEE), GUANGJIE HAN[3], JINGPENG LIANG[1], RONG DAI[1], AND ZHENG-QUAN LI[1,4]

[1]School of Internet of Things Engineering, Jiangnan University, Wuxi 214122, China
[2]Key Laboratory of Wireless Communication of Jiangsu Province, Nanjing University of Posts and Telecommunication, Nanjing 210003, China
[3]Key Laboratory for Ubiquitous Network and Service Software of Liaoning Province, School of Software, Dalian University of Technology, Dalian 116024, China
[4]State Key Laboratory of Networking and Switching Technology, Beijing University of Posts and Telecommunications, Beijing 100876, China

Corresponding author: Guangjie Han (hanguangjie@gmail.com)

This work was supported in part by the National Natural Science Foundation of China under Grant 61801193, Grant 61871233, Grant 61871446, and Grant 61571108, in part by the Open Foundation of Key Laboratory of Wireless Communication, Nanjing University of Posts and Telecommunication under Grant 2017WICOM01, in part by the Open Foundation of State Key Laboratory of Millimeter Waves, Southeast University under Grant K201918, and in part by the Open Foundation of State Key Laboratory of Networking and Switching Technology, Beijing University of Posts and Telecommunications under Grant SKLNST-2016-2-14.

ABSTRACT A novel frequency-dependent wall insertion loss model at 3–6 GHz is proposed in this paper. The frequency-dependence of the wall insertion loss is modeled by the Fourier triangular basis neural network. A method to determine the optimal weighted vector and the number of the neurons is introduced. In addition, the impact of the wider continuous spectrum on the wall insertion loss is analyzed and extensive measurements are performed to validate the proposed model. The results obtained with the proposed model match better with the measured results than other models. The proposed model can be used in future indoor Internet-of-Things applications such as service computing.

INDEX TERMS Wall insertion loss, neural network, 3-6 GHz, internet of things (IoT).

I. INTRODUCTION

As one of the key technologies in future wireless communication system, the internet of things (IoT) will gradually be integrated into daily life [1]. Service computing plays an important role in the IoT applications [2]. Through the information interaction between a huge number of devices and the computing among various services, the IoT can provide various kinds of smart applications [3], [4]. Among them, indoor services such as personal healthcare and smart home, are typical services provided by the IoT. Understanding the indoor propagation characteristics is very important for constructing the indoor IoT [5]. However, the densely and randomly distributed walls under the indoor environment makes the propagation properties much more complex. Accordingly, only modeling the wall insertion loss correctly can offer several useful options for the follow-up work, such as wireless coverage and interference suppression.

Towards this objective, various wall insertion models have been proposed in the past few decades. In general, these models can be classified into the material-dependent, angle-dependent and thickness-dependent models. In the material-dependent model, the wall insertion loss for typical materials, such as brick, glass, concrete, has been measured and analyzed [6]–[8]. In the angle-dependent model, the influence of the angle of incidence on the wall insertion loss has also been measured and analyzed [9], [10]. The thickness-dependent model indicates that the wall insertion loss in decibel has a linear relationship with the thickness [8], [11].

Basically, the above studies mainly focused on studying the wall insertion loss over the narrowband spectrum. Thus, the frequency dependence of the wall insertion loss was not considered in those studies. In the future IoT systems, a wider continuous spectrum may be allocated and a general, empirical, frequency-dependent wall insertion loss model may be more useful. In a previous study [12], the experimental results showed that the expectation of the wall insertion has a linear relationship with the frequency. However, the wall insertion loss may fluctuate significantly over such wider spectrum due to the inhomogeneity of the sampled wall. Thus, the wall insertion loss may show a complex and non-linear relationship with the frequency. Unfortunately, traditional algebraic approaches may not describe this frequency-dependence accurately. Therefore, it is a challenging task to develop a frequency-dependent wall insertion loss model.

In this situation, the neural network (NN) may play a substantial role in learning the complex non-linear dependence. Previous studies have shown that the NN can approximate any nonlinear function with lower estimated errors [13]–[16]. Motivated by the need of future indoor IoT systems, a novel NN-based frequency-dependent wall insertion loss model is proposed in this paper. The main contributions of this paper are the following:

- A novel, empirical, frequency-dependent wall insertion loss model based on a NN is proposed in this paper. The frequency-dependence of the wall insertion loss is fitted by a NN with the Fourier triangular basis. The formula to calculate the optimal weighted vector is derived and the procedure to determine the number of neurons in the hidden layer is introduced. Then the algorithm for simulating the wall insertion loss at each discrete frequency is given. Extensive measurements are performed to validate the proposed model. Compared with the linear model, the results obtained with our proposed model match better with the measured results. Compared with the back propagation (BP) NN method, our proposed model has faster calculation speed to achieve approximation performances.
- The impact of the wider continuous spectrum on the parameters and the wall insertion loss are analyzed. The results show that the m-parameters have no significant correlation with the frequency but the Ω parameters show a declined trend with the frequency. In addition, the wall insertion loss will rise with the frequency and fluctuate significantly during the rise.
- In order to verify the universality of the proposed model, we perform extensive measurements at another similarly sampled wall. The measured wall insertion loss is compared with the ones predicted by the proposed model. The results demonstrate the accuracy and universality of the proposed frequency-dependent model for predicting the wall insertion loss.

The rest of this paper is organized as follows. The NN-based frequency-dependent wall insertion loss model is proposed in Section II. The measurement environment and setup are described in Section III. The analysis of the modeling results and validation of the universality of the proposed model are presented in Section IV. The conclusions drawn from this study are given in Section V.

II. NN-BASED FREQUENCY-DEPENDENT WALL INSERTION LOSS MODEL

In this section, a novel NN-based frequency-dependent wall insertion loss model is proposed. A Nakagami fading channel is assumed to describe the statistical properties of the wall insertion loss [17].

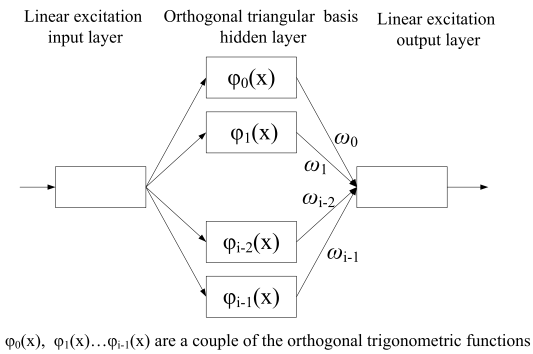

FIGURE 1. the structure of NN for modeling the frequency-dependence of the parameters.

A. PROPOSED MODEL

The wall insertion loss (dimensionless) is defined as the ratio of the instantaneous power in the absence (abs-link) and presence (pre-link) of the wall [18]. Previous studies have shown that the wall insertion loss over a Nakagami fading channel has a generalized beta prime distribution [19]. The probability distribution function (PDF) of the wall insertion is expressed as

$$f_{W_{loss}}(x) = \frac{(x \cdot \frac{\Omega_2}{\Omega_1} \cdot \frac{m_1}{m_2})^{m_1-1}(1 + x \cdot \frac{\Omega_2}{\Omega_1} \cdot \frac{m_1}{m_2})^{-m_1-m_2}}{\frac{\Omega_1}{\Omega_2} \cdot \frac{m_2}{m_1} B(m_1, m_2)} \tag{1}$$

where m_1, Ω_1 and m_2, Ω_2 are the frequency-dependent parameters of the abs-link and pre-link respectively.

Then we use a NN with the Fourier triangular basis to model the frequency-dependence of the parameters. The structure of the Fourier triangular basis NN is shown in Fig.1, where the activation functions of the hidden layer are a couple of the orthogonal trigonometric functions. The Fourier triangular basis NN is constructed based on the fact that a sum of the orthogonal trigonometric functions can approximate to any objective function at the interval $[a, b]$ [16].

$$y(x) \approx \sum_{i=0}^{N-1} \omega_i \varphi_i(x) \tag{2}$$

$$\varphi_i(x) = \begin{cases} 1, & i = 0 \\ \cos[(i+1) \cdot \frac{\pi}{2(b-a)} x), & i = 1, 3, 5, \cdots \\ \sin(i \cdot \frac{\pi}{2(b-a)} x), & i = 2, 4, 6 \cdots \end{cases} \tag{3}$$

We use the following function to define the error between the objective and approximated functions

$$e = \frac{1}{2} \sum_{j=1}^{M} [y(x_j) - y_{sim}(x_j)]^2 \tag{4}$$

$$y_{sim}(x) = \sum_{i=0}^{N-1} \omega_i \varphi_i(x) \tag{5}$$

where $y(x_j)$ and $y_{sim}(x_j)$, $(j = 1, \ldots M)$, represent each sample of the objective and approximated functions, respectively.

Thus, the objective of the NN is to find the optimal weighted vector $\boldsymbol{\omega}^* = \left(\omega_0^* \; \omega_1^* \; \cdots \; \omega_{N-1}^*\right)$ corresponding to the minimum error e_{min}.

The typical training algorithm, such as Levenberg-Marquardt and Bayesian regularization [16] can achieve the optimal weighted vector $\boldsymbol{\omega}^*$ by many iterations. However, these iterations cost plenty of training time. To avoid the lengthy iterated process, we can obtain the optimal weighted vector $\boldsymbol{\omega}^*$ directly as follows:

$$\boldsymbol{\omega}^* = (\boldsymbol{X}^T\boldsymbol{X})^{-1}\boldsymbol{X}^T\boldsymbol{Y} \tag{6}$$

$$\boldsymbol{X} = \begin{pmatrix} \varphi_0(x_1) & \varphi_1(x_1) & \cdots & \varphi_{N-1}(x_1) \\ \varphi_0(x_2) & \varphi_1(x_2) & \cdots & \varphi_{N-1}(x_2) \\ \vdots & \vdots & \vdots & \vdots \\ \varphi_0(x_M) & \varphi_1(x_M) & \cdots & \varphi_{N-1}(x_M) \end{pmatrix} \tag{7}$$

$$\boldsymbol{Y} = \left(y(x_1) \; y(x_2) \; \cdots \; y(x_M)\right)^T \tag{8}$$

where $\boldsymbol{X}$ and $\boldsymbol{Y}$ are defined as the eigen matrix and objective vector, respectively. $(\cdot)$ represents the transpose of the matrix.

Proof: The NN uses the gradient descent algorithm to find the optimal weighted vector $\boldsymbol{\omega}^*$. The iterative formula of the weighted coefficients can be expressed as

$$\omega_i(l+1) = \omega_i(l) - \eta \frac{\partial e}{\partial \omega_i} \tag{9}$$

where η is defined as the learning rate.

Substituting (4) and (5) into (9), we can get

$$\omega_i(l+1) = \omega_i(l) - \eta \sum_{j=1}^{M} \{[\sum_{p=0}^{N-1} \omega_p(l)\varphi_p(x_j) - y(x_j)]\varphi_i(x_j)\} \tag{10}$$

In matrix form, equation (10) can be expressed as:

$$\boldsymbol{\omega}(l+1) = \boldsymbol{\omega}(l) - \eta\boldsymbol{X}^T[\boldsymbol{X}\boldsymbol{\omega}(l) - \boldsymbol{Y}] \tag{11}$$

where the matrix $\boldsymbol{X}$ and $\boldsymbol{Y}$ are defined as equations (7) and (8), respectively.

The vector $\boldsymbol{\omega}(l)$ is the weighted vector obtained from the l^{th} iterative step.

$$\boldsymbol{\omega}(l) = \left(\omega_0(l) \; \omega_1(l) \; \cdots \; \omega_{N-1}(l)\right)^T \tag{12}$$

Thus, the optimal weighted vector $\boldsymbol{\omega}^*$ can be obtained by taking the limit of both sides in (11).

$$\boldsymbol{\omega}^* = \lim_{l\to\infty} \boldsymbol{\omega}(l) = (\boldsymbol{X}^T\boldsymbol{X})^{-1}\boldsymbol{X}^T\boldsymbol{Y} \tag{13}$$

Therefore, the optimal weighted vector of each parameter can be estimated according to equation (6). ∎

Next, the number of neurons in the hidden layer needs to be determined. The fitting may not be the best if the number of neurons is too low. On the other hand, overfitting may occur when the number of neurons is too large. Therefore, the number of neurons plays an important role in a NN. In this paper, the number of neurons is determined through the procedure depicted in Fig. 2.

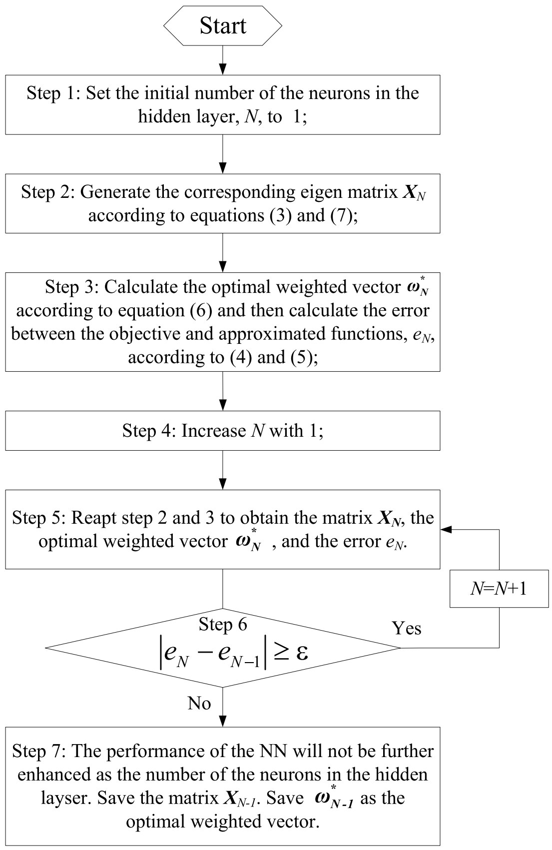

FIGURE 2. The flowchart of the method to determine the number of neurons in the hidden layer.

B. PARAMETERS EXTRACTION

The algorithm for extracting the parameters m_1, m_2, Ω_1, Ω_2 at each frequency can be expressed as

$$m_{1k} = E^2(P_k^{abs})/Var(P_k^{abs}) \tag{14}$$
$$\Omega_{1k} = E(P_k^{abs}) \tag{15}$$
$$m_{2k} = E^2(P_k^{pre})/Var(P_k^{pre}) \tag{16}$$
$$\Omega_{2k} = E(P_k^{pre}) \tag{17}$$

where P_k^{abs} and P_k^{pre} are the instantaneous power of the abs-link and pre-link at each frequency, respectively.

To obtain a consistent threshold when determining the number of the neurons, all the parameters are normalized as

$$\bar{m}_{1j} = \frac{m_{1j} - \min(m_1)}{\max(m_1) - \min(m_1)} \tag{18}$$
$$\bar{\Omega}_{1j} = \frac{\Omega_{1j} - \min(\Omega_1)}{\max(\Omega_1) - \min(\Omega_1)} \tag{19}$$
$$\bar{m}_{2j} = \frac{m_{2j} - \min(m_2)}{\max(m_2) - \min(m_2)} \tag{20}$$
$$\bar{\Omega}_{2j} = \frac{\Omega_{2j} - \min(\Omega_2)}{\max(\Omega_2) - \min(\Omega_2)} \tag{21}$$

where $\min(\cdot)$ and $\max(\cdot)$ are the functions to calculate the maximum and minimum values over all the samples of each parameter.

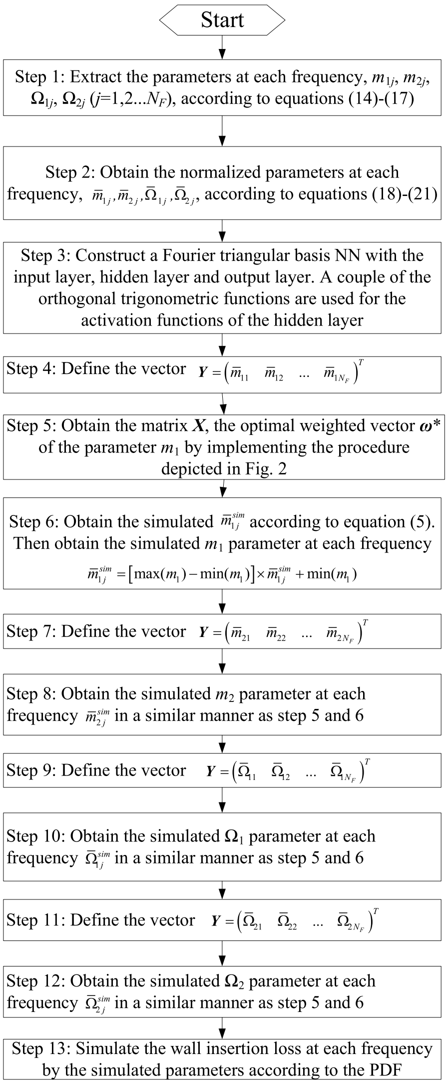

FIGURE 3. the flowchart of generating the wall insertion loss.

C. PARAMETERS EXTRACTION

The simulated procedure for the wall insertion loss is depicted in Fig. 3 . First, the parameters at each frequency are extracted from the measured data. Then a Fourier triangular basis NN is set up. The number of neurons in the hidden layer is determined through the procedure depicted in Fig. 2. Next, each parameter is simulated according to its own optimal weighted vector. Eventually, the wall insertion loss at each frequency is generated according to the PDF of the wall insertion loss.

III. MEASUREMENT SETUP

Extensive measurements are performed to determine the accuracy of the proposed model. In theory, the measurements should be conducted in an anechoic chamber. However, the experimental conditions do not allow us to perform the measurements in a microwave anechoic chamber. In the previous studies, several wall insertion loss measurements were performed under different environments. These studies showed that the approximate results could also be achieved if an approximated sampled wall was chosen [6], [9], [12].

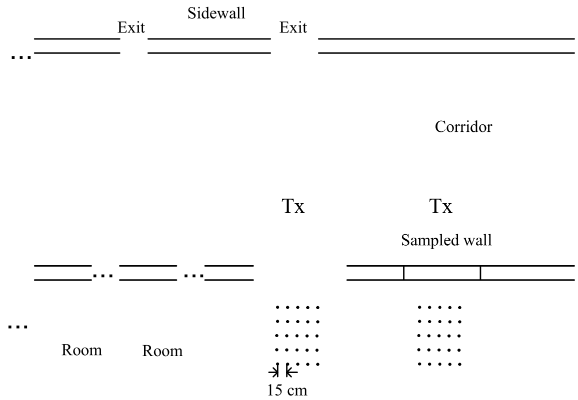

FIGURE 4. The layout of the environment.

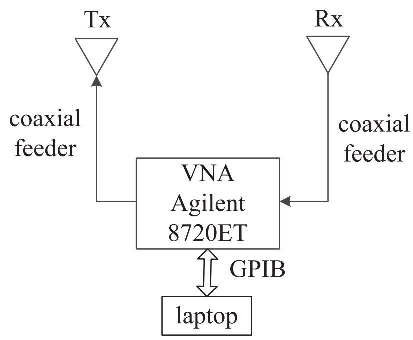

FIGURE 5. Block diagram of frequency-domain measurement system.

A. ENVIRONMENT

In this study, the measurements are performed in a corridor in an office building. We choose a concrete wall with 17-cm thickness to perform the measurement. The sampled wall is large enough that the diffracted wave can be ignored [20]. The sampled wall is 4 m away from the sided wall. During the measurements, there are no the other objects or persons. The layout of the measured environment is depicted in Fig. 4.

B. MEASUREMENT SYSTEM

A frequency-domain measurement is performed using the Agilent 8720ET vector network analyzer (VNA), as shown in Fig. 5 [21]. The VNA generates a 10-dBm, 151-point sweeping signal from 3-6 GHz. The synchronization between the transmitted and received signal is achieved through a 15m-long coaxial feeder. Both the transmitter and receiver antennas are isotropic and vertical polarized antennas fixed at a height of 1.5 m. The gain of each antenna is 3 dBi. The measurement data are transmitted to the laptop computer through a GPIB interface. The calibration of this system is performed by the electronic calibration module. A higher dynamic range and lower noise level can be achieved with this measurement system.

TABLE 1. Number of neurons in the hidden layer for each parameter.

parameter	m_1	m_2	Ω_1	Ω_2
number	14	12	14	8

C. MEASUREMENT PROCEDURE

First, the frequency response in the absence of the wall is measured to establish a reference. Then we measure the frequency response in the presence of the sampled wall. The Tx-Rx distance is the same as that of the reference measurement and large enough to ensure that the sampled wall is in the far field. Both measurements are performed at 5×5 grids and the interval between the adjacent interval is 15 cm. At each grid, the measurements are repeated 8 times to reduce the noise.

IV. MODELING RESULTS

A. MODEL PARAMETERS EXTRACTION

The measured wall insertion loss at each discrete frequency point $f_i (i = 1...151)$ is computed as previously reported [6], as follows:

$$IL(f_i) = 10\log_{10}\frac{1}{200}\sum_{j=1}^{8}\sum_{k=1}^{25}\left|H_{ref}(t_j, g_k; f_i)\right|^2 - 10\log_{10}\frac{1}{200}\sum_{j=1}^{8}\sum_{k=1}^{25}\left|H(t_j, g_k; f_i)\right|^2 \quad (22)$$

where $H(t_j, g_k; f_i)$ and $H_{ref}(t_j, g_k; f_i)$ are the measured frequency responses of the pre-link and abs-link, respectively; $t_j (j = 1...8)$ stands for the temporal samples; $g_k (k = 1...25)$ stands for the sample at each grid.

Then, we can extract the parameters of the pre-link and abs-link from the measured frequency responses according to the equations (14)-(17).

B. NUMBER OF NEURONS IN THE HIDDEN LAYER

For each parameter, the number of neurons is determined by following the steps in Section II, subsection A. The results are summarized in Table 1. Only the parameter Ω_2 needs the lower number of neurons. Then we save the error and the optimal weighted vector corresponding to each parameter.

C. CORRELATION OF THE PARAMETERS WITH THE FREQUENCIES

Using the optimal weighted vector, we can simulate the parameter at each input frequency. The parameters against the frequencies are depicted in Fig. 6-9. Specifically, in Fig. 6 and 7, the m-parameters of both links show no significant correlation with frequency because the m-parameter depends mainly on the propagation environment. Besides, the m_2 parameter is larger than 1 at several frequencies since the principal component is even present in the pre-link. Furthermore, the results shown in Fig. 8 and 9 indicate that the

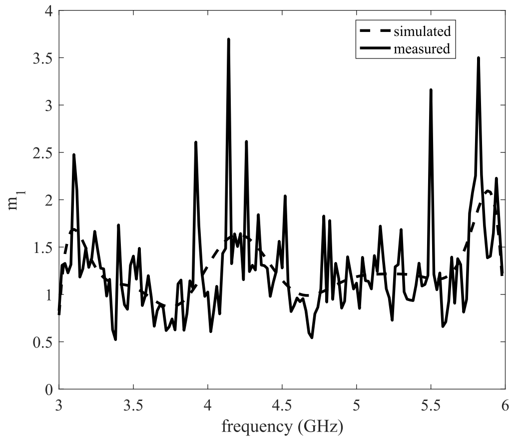

FIGURE 6. The frequency dependence of parameter m_1.

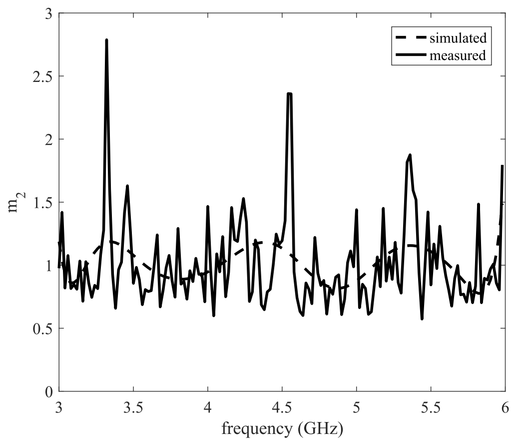

FIGURE 7. The frequency dependence of parameter m_2.

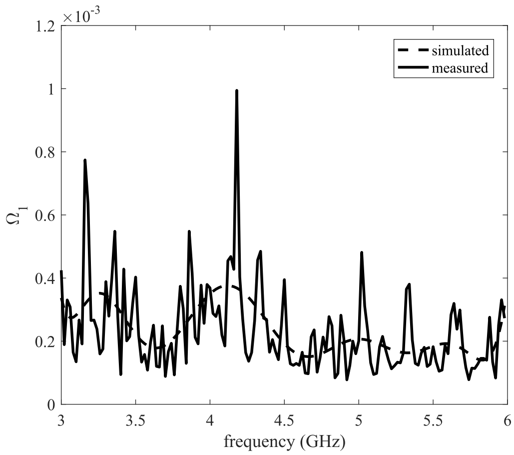

FIGURE 8. The frequency dependence of parameter Ω_1.

Ω_1 and Ω_2 parameters show a declined trend with the frequency as a result of the increased power loss.

D. FREQUENCY-DEPENDENCY OF THE WALL INSERTION LOSS

The simulated and measured wall insertion loss versus the frequency are shown in Fig. 10-Fig.12. Since the modeled

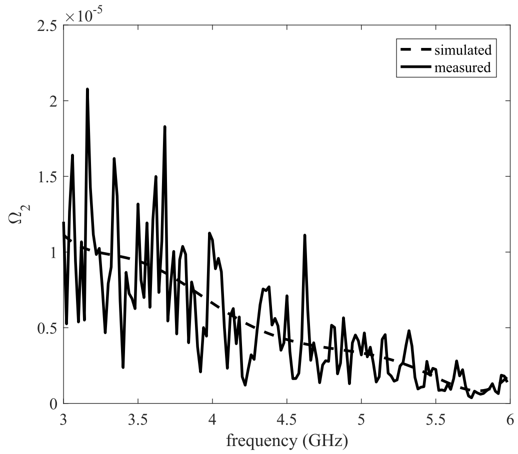

FIGURE 9. The frequency dependence of parameter Ω_2.

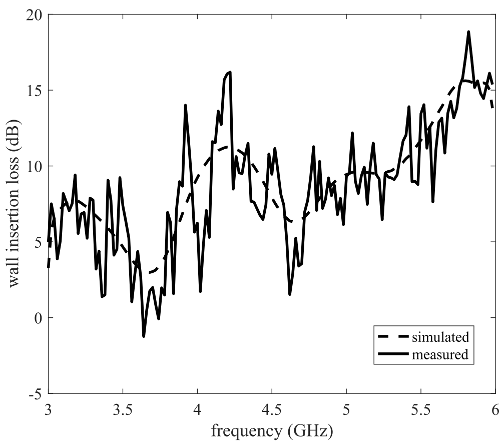

FIGURE 10. The measured and fitted wall insertion loss versus the frequency at 10% quantile.

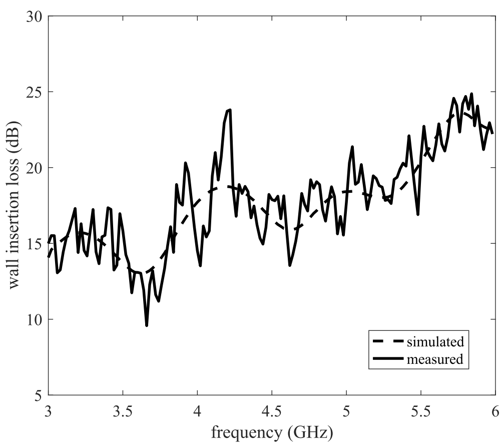

FIGURE 11. The measured and fitted wall insertion loss versus the frequency at 50% quantile.

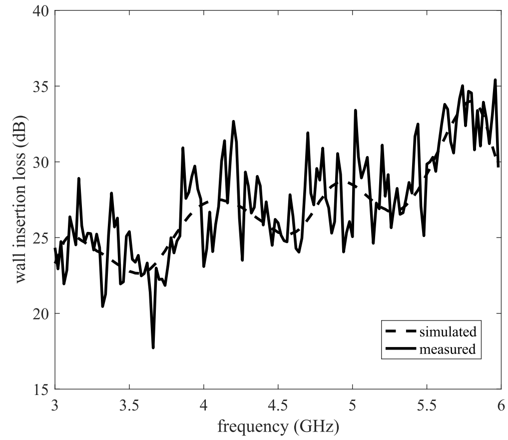

FIGURE 12. The measured and fitted wall insertion loss versus the frequency at 90% quantile.

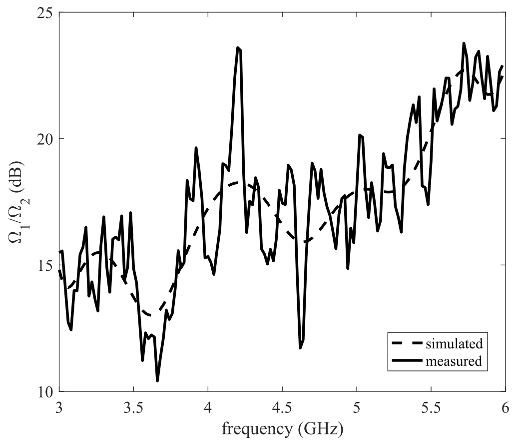

FIGURE 13. The measured and fitted Ω_1/Ω_2 versus the frequency.

and measured cumulative distribution functions (CDFs) at each discrete frequency point cannot be clearly graphically depicted, we choose the 10%, 50%, 90% quantile at each frequency. Previous studies indicate that the wall insertion loss is mainly determined by the ratio of the parameter Ω_1 and Ω_2. Then, the ratio of the parameter Ω_1 and Ω_2 versus the frequency is shown in Fig.13. These results reveal that the ratio of the parameters Ω_1 and Ω_2 show an uptrend with the frequency. Thus, as seen in Fig.10-Fig.12, the wall insertion loss rise with the frequency due to the increased Ω_1/Ω_2. However, due to the inhomogeneity of the sampled wall, the wall insertion loss will fluctuate significantly during the rise.

E. COMPARED WITH OTHER MODELS

In a previous study [12], the expectation of the wall insertion loss was found to be linearly correlated with the frequency. Therefore, we compare the proposed model with the linear model so as to obtain a scientific quantification of the performance. In the linear model, the wall insertion loss against the frequency can be expressed as previously reported [12]:

$$I_{loss} = a_{I_{loss}} f + b_{I_{loss}} \tag{23}$$

Then we can estimate $a_{I_{loss}}$ and $b_{I_{loss}}$ from the measured data and simulate the wall insertion using the linear model.

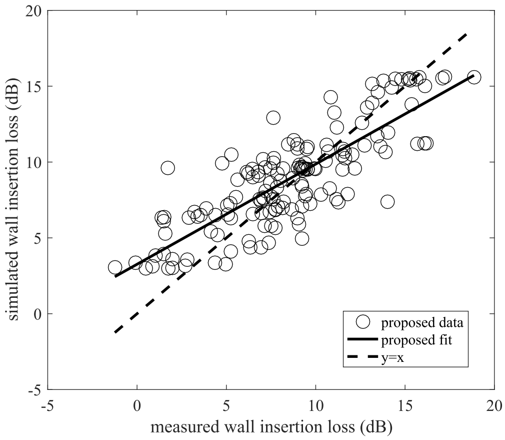

FIGURE 14. **The proposed modeled wall insertion loss versus the measured results at 10% quantile.**

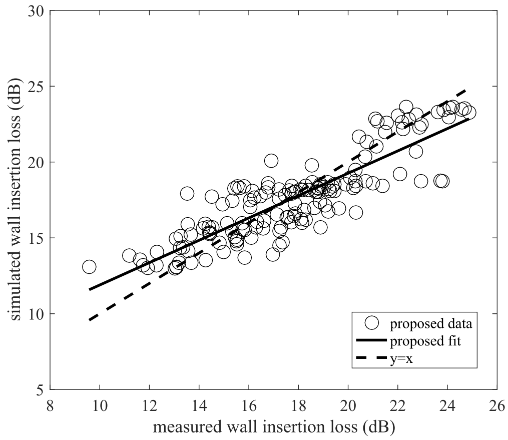

FIGURE 16. **The proposed modeled wall insertion loss versus the measured results at 50% quantile.**

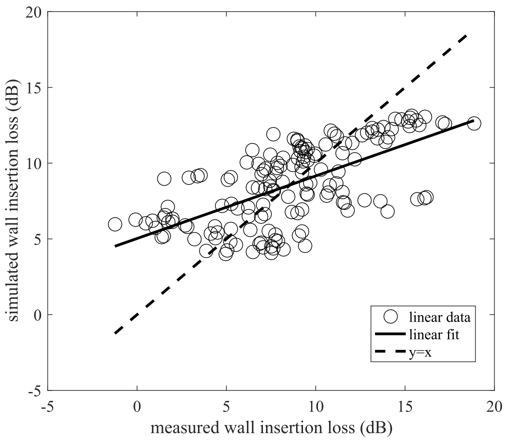

FIGURE 15. **The linear modeled wall insertion loss versus the measured results at 10% quantile.**

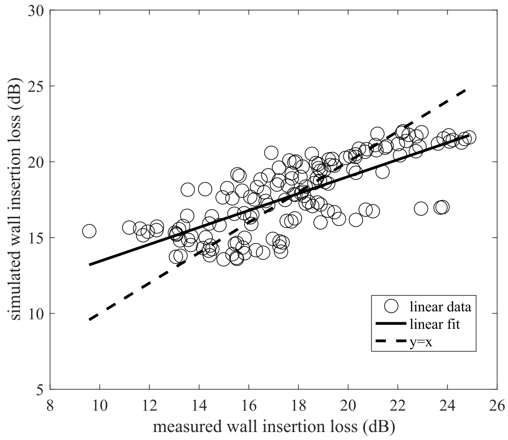

FIGURE 17. **The linear modeled wall insertion loss versus the measured results at 50% quantile.**

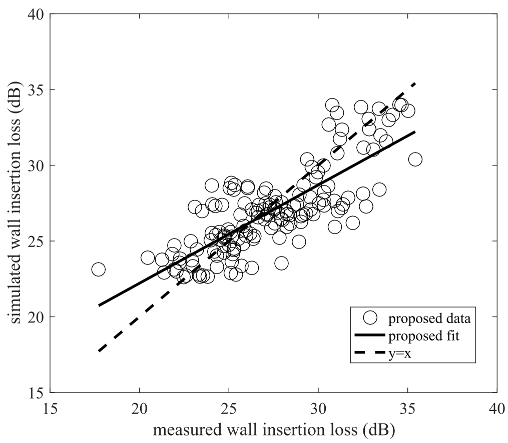

FIGURE 18. **The proposed modeled wall insertion loss versus the measured results at 90% quantile.**

Each of the simulated wall insertion loss from the proposed model and linear model versus the measured results at each quantile are displayed in Fig.14-19. The R-square values and the fitting functions at each quantile are summarized in Table 2-4. The R-square value indicates the fitting performance between the simulated and measured results. The fitting with R-square = 1 is a perfect fitting. The nearer the fitting function approximates to the function $y = x$, the better the fitting is. As shown in Table 2-4, the proposed method is more accurate for modeling the wall insertion loss than the linear method.

In this paper, we also use a typical BP NN to model the frequency-dependence of the wall insertion loss [16]. The NN still includes three layers, namely the input layer, hidden layer, and output layer. The sigmoid function is used for the activation function of the hidden layer. The number of neurons in the hidden layer is the same as that in the Fourier triangular basis NN. Bayesian regularization training algorithm is used to train the NN.

The results obtained from the BP method are displayed in Fig. 20-22 The modeled results are compared with those of the proposed model, as shown in Table 5. The comparison shows that the proposed model requires less computational time to achieve the approximation performances compared with the BP method. This demonstrates that the proposed

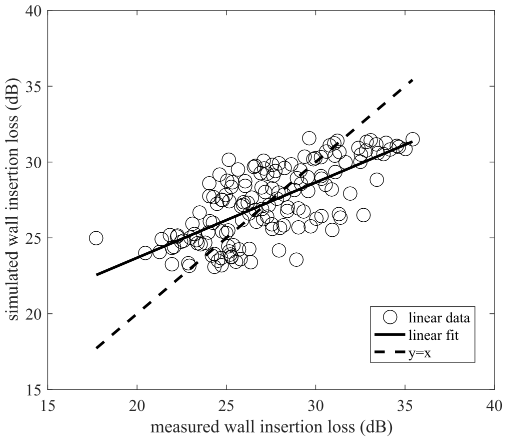

FIGURE 19. The linear modeled wall insertion loss versus the measured results at 90% quantile.

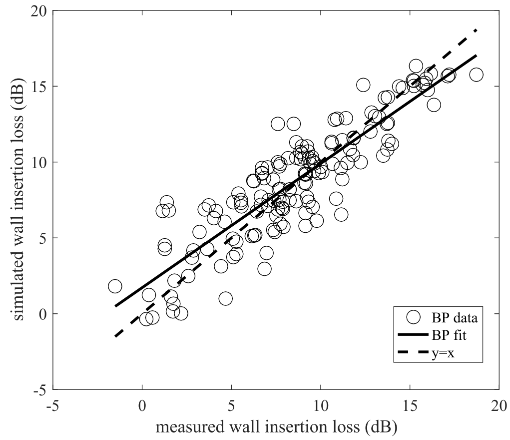

FIGURE 20. The wall insertion loss obtained from the BP method versus the measured results at 10% quantile.

TABLE 2. The R-square values and the fitting functions of the proposed and the linear model at 10% quantile.

	Proposed model	Linear model
R-square	0.67	0.41
fitting function	$y = 0.66x + 3.26$	$y = 0.41x + 4.92$

TABLE 3. The R-square values and the fitting functions of the proposed and the linear model at 50% quantile.

	Proposed model	Linear model
R-square	0.75	0.55
fitting function	$y = 0.74x + 4.52$	$y = 0.56x + 7.90$

TABLE 4. The R-square values and the fitting functions of the proposed and the linear model at 90% quantile.

	Proposed model	Linear model
R-square	0.63	0.50
fitting function	$y = 0.65x + 9.20$	$y = 0.49x + 13.80$

TABLE 5. The computational time and R-square values of the proposed method and BP method.

	proposed model			BP method		
time	0.023s			4.5s		
R-square	10%	50%	90%	10%	50%	90%
	0.67	0.75	0.63	0.77	0.80	0.63

model is more effective because it does not require the lengthy iterative process.

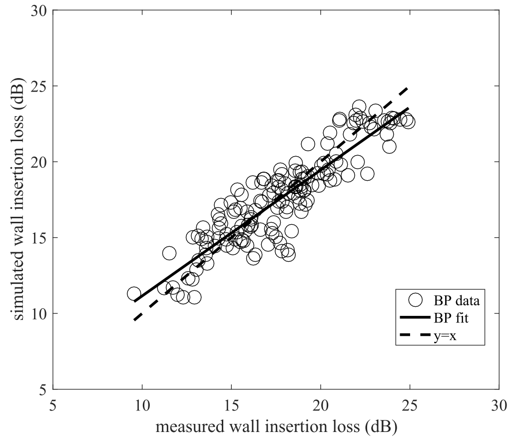

FIGURE 21. The wall insertion loss obtained from the BP method versus the measured results at 50% quantile.

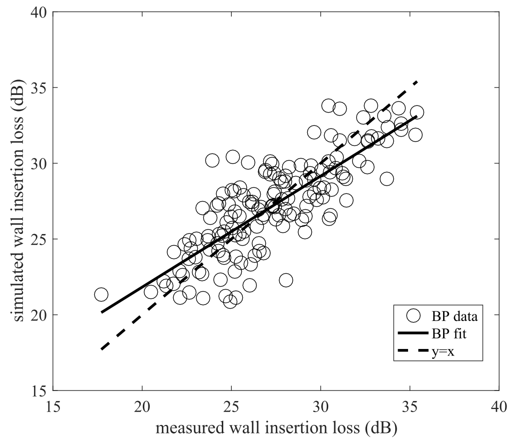

FIGURE 22. The wall insertion loss obtained from the BP method versus the measured results at 90% quantile.

F. VALIDATION OF THE UNIVERSALITY OF THE PROPOSED MODEL

In order to validate the universality of the proposed wall insertion loss model, we perform measurements at another similarly sampled wall. This sampled wall is also made of concrete with a thickness of 17 cm. The sampled wall is also large enough so as to ignore the diffracted wave. Then, we use the proposed model to predict the wall insertion loss and compare the predicted results with the measured data. The predicted wall insertion loss versus the measured ones are shown in Fig. 23-25 The R-square values at the

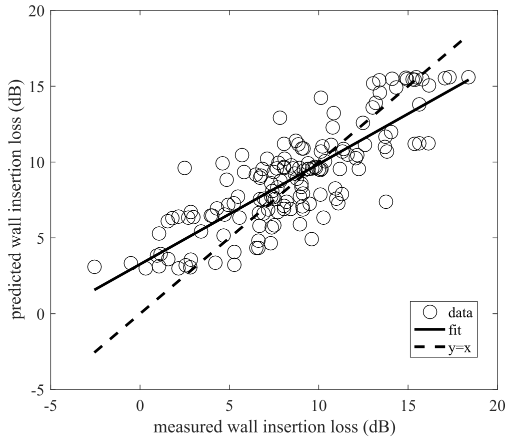

FIGURE 23. the predicted wall insertion loss versus the measured results at 10% quantile.

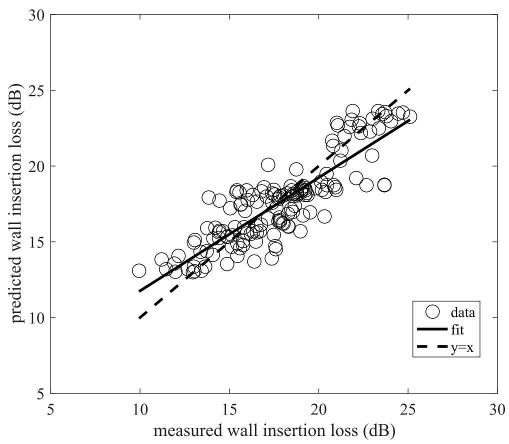

FIGURE 24. the predicted wall insertion loss versus the measured results at 50% quantile.

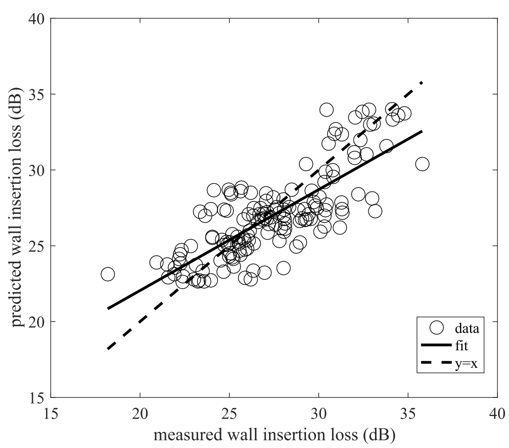

FIGURE 25. the predicted wall insertion loss versus the measured results at 90% quantile.

three quantiles are 0.6720, 0.7445, 0.6016 respectively. These results demonstrate the accuracy and universality of the proposed frequency-dependent model for predicting the wall insertion loss.

G. APPLICATION OF THE PROPOSED MODEL

The proposed wall insertion loss model can be employed in future indoor IoT applications. For example, it can be used in service computing when a link budget is required. The attenuation caused by the interior wall can be estimated by the proposed model and the link budget under the indoor propagation environment with random distributed walls will be more accurate. Thus, the service computing will be more effective.

In addition, this model can be expanded to be multi-dimensional. Since the wall insertion loss may be affected by several factors such as the frequency, thickness, material, a multi-dimensional model based on the NN algorithm will be feasible and useful.

Furthermore, we can also study other methods to further enhance the fitting performances. For example, we can design the NN with different orthogonal basis functions and try to calculate the optimal weighted vector with these orthogonal basis functions. Additionally, we can explore the other optimization methods to determine the optimal weighted vector.

V. CONCLUSION

In this paper, an empirical frequency-dependent wall insertion loss model at $3-6$ GHz is proposed for IoT applications. A Fourier triangular basis NN is used to model the frequency-dependence of the distributed parameters of the wall insertion loss. The optimal weighted vector is given directly and the algorithm to determine the number of neurons in the hidden layer is introduced.

Extensive wall insertion loss measurements are performed to validate the proposed model. The m-parameters show no significant correlation with the frequency and most of them are larger than 1 due to the principal component. On the other hand, the Ω parameters show a fluctuating and declining trend with the frequency. Furthermore, the wall insertion loss will rise with the frequency as a result of the increased ratio of the parameters Ω_1 and Ω_2.

To obtain a scientific quantification of the performance, the proposed method is compared with method involving the linear model and the BP algorithm. The R-square values and the fitting function indicate that the proposed model is more accurate than the linear model. Moreover, the proposed model requires the less computational time to achieve the approximation performances compared with the BP model. This finding demonstrates that the proposed model is more effective.

In order to confirm the universality of the proposed wall insertion loss model, we perform extensive measurements at another similarly sampled wall. We use the proposed model to predict the insertion loss at this sampled wall and compare it with the measured results. The R-square values between the predicted and measured results demonstrate the effectiveness and universality of the proposed frequency-dependent model for predicting the wall insertion loss.

The proposed wall insertion loss model can be employed in future indoor IoT applications, such as the link budget, network optimization and the evaluation of electromagnetic interference. Furthermore, this model can be expanded to be multi-dimensional.

ACKNOWLEDGMENT
The authors are indebted to the employees of the China Academy of Telecommunication Research of MIIT (CAICT), for their assistance in the wall insertion loss measurements.

REFERENCES
[1] S. Sharma, A. Gupta, and V. Bhatia, "IR-UWB sensor network using massive MIMO decision fusion: Design and performance analysis," *IEEE Sensors J.*, vol. 18, no. 15, pp. 6290–6302, Aug. 2018.
[2] Y. Zhang, J. Li, Z. Zhou, and X. Liu, "Efficient dynamic service maintenance for edge services," *IEEE Access*, vol. 6, pp. 8829–8840, Feb. 2018.
[3] M. R. Rahimi, N. Venkatasubramanian, S. Mehrotra, and A. V. Vasilakos, "On optimal and fair service allocation in mobile cloud computing," *IEEE Trans. Cloud Comput.*, vol. 6, no. 3, pp. 815–828, Sep. 2018.
[4] F. Tang, B. Mao, Z. M. Fadlullah, and N. Kato, "On a novel deep-learning-based intelligent partially overlapping channel assignment in SDN-IoT" *IEEE Commun. Mag.*, vol. 56, no. 9, pp. 80–86, Sep. 2018.
[5] A. Burg, A. Chattopadhyay, and K.-Y. Lam, "Wireless communication and security issues for cyber–physical systems and the Internet-of-Things," *Proc. IEEE*, vol. 106, no. 1, pp. 38–60, Jan. 2018.
[6] I. Cuinas and M. G. Sanchez, "Measuring, modeling, and characterizing of indoor radio channel at 5.8 GHz," *IEEE Trans. Veh. Technol.*, vol. 50, no. 2, pp. 526–535, Mar. 2001.
[7] C.-F. Yang, B.-C. Wu, and C.-J. Ko, "A ray-tracing method for modeling indoor wave propagation and penetration," *IEEE Trans. Antennas Propag.*, vol. 46, no. 6, pp. 907–919, Jun. 1998.
[8] N. Moraitis and P. Constantinou, "Indoor channel measurements and characterization at 60 GHz for wireless local area network applications," *IEEE Trans. Antennas Propag.*, vol. 52, no. 12, pp. 3180–3189, Dec. 2004.
[9] D. Pena, R. Feick, H. D. Hristov, and W. Grote, "Measurement and modeling of propagation losses in brick and concrete walls for the 900-MHz band," *IEEE Trans. Antennas Propag.*, vol. 51, no. 1, pp. 31–39, Jan. 2003.
[10] J. Horikoshi, K. Tanaka, and T. Morinaga, "1.2 GHz band wave propagation measurements in concrete building for indoor radio communications," *IEEE Trans. Veh. Technol.*, vol. VT-35, no. 4, pp. 146–152, Nov. 1986.
[11] G. Hwang, K. Shin, S. Park, and H. Kim, "Measurement and comparison of Wi-Fi and super Wi-Fi indoor propagation characteristics in a multi-floored building," *J. Commun. Netw.*, vol. 18, no. 3, pp. 476–483, Jun. 2016.
[12] T. M. Schafer, J. Maurer, J. von Hagen, and W. Wiesbeck, "Experimental characterization of radio wave propagation in hospitals," *IEEE Trans. Electromagn. Compat.*, vol. 47, no. 2, pp. 304–311, May 2005.
[13] S. K. Gharghan, R. Nordin, M. Ismail, and J. A. Ali, "Accurate wireless sensor localization technique based on hybrid PSO-ANN algorithm for indoor and outdoor track cycling," *IEEE Sensors J.*, vol. 16, no. 2, pp. 529–541, Jan. 2016.
[14] H. Chen, Y. Zhang, W. Li, X. Tao, and P. Zhang, "ConFi: Convolutional neural networks based indoor Wi-Fi localization using channel state information," *IEEE Access*, vol. 5, pp. 18066–18074, 2017.
[15] G. P. Ferreira, L. J. Matos, and J. M. M. Silva, "Improvement of outdoor signal strength prediction in UHF band by artificial neural network," *IEEE Trans. Antennas Propag.*, vol. 64, no. 12, pp. 5404–5410, Dec. 2016.
[16] S. O. Haykin, *Neural Networks and Learning Machines*. Upper Saddle River, NJ, USA: Prentice-Hall, 2008.
[17] W. Braun and U. Dersch, "A physical mobile radio channel model," *IEEE Trans. Veh. Technol.*, vol. 40, no. 2, pp. 472–482, May 1991.
[18] T. B. Gibson and D. C. Jenn, "Prediction and measurement of wall insertion loss," *IEEE Trans. Antennas Propag.*, vol. 47, no. 1, pp. 55–57, Jan. 1999.
[19] Y. Liu, Y. Yu, Q. Wu, Z.-Q. Li, W.-J. Lu, and H.-B. Zhu, "A closed-form and stochastic wall insertion loss model for dense small cell networks," *IEEE Access*, vol. 6, pp. 11596–11604, Jan. 2018.
[20] A. Muqaibel, A. Safaai-Jazi, A. Bayram, A. M. Attiya, and S. M. Riad, "Ultrawideband through-the-wall propagation," *Proc. IEE Microw., Antennas Propag.*, vol. 152, no. 6, pp. 581–588, Dec. 2005.
[21] Y. Yu, P.-F. Cui, W.-J. Lu, Y. Liu, and H.-B. Zhu, "Off-body radio channel impulse response model under hospital environment: Measurement and modeling," *IEEE Commun. Lett.*, vol. 20, no. 11, pp. 2332–2335, Nov. 2016.

YANG LIU (M'18) was born in Wuxi, Jiangsu, China, in 1988. He received the Ph.D. degree in communication and information system from the Key Laboratory of Wireless Communication, Nanjing University of Posts and Telecommunications, Nanjing, China, in 2016. He is currently a Lecture with the Institute of IoT Engineering, Jiangnan University, Wuxi. He has authored or co-authored over 10 technical papers published in peer-reviewed international journals and conference proceedings, including the IEEE Access, and the IEEE CL. His current research interests include wireless channel modeling and network coding.

GUANGJIE HAN (S'03–M'05–SM'18) received the Ph.D. degree from Northeastern University, Shenyang, China, in 2004. From 2004 to 2005, he was a Product Manager with the ZTE Company. From 2005 to 2006, he was the Key Account Manager for Huawei Co., Ltd.. In 2008, he finished his work as a Post-Doctoral Researcher with the Department of Computer Science, Chonnam National University, Gwangju, South Korea. From 2010 to 2011, he was a Visiting Research Scholar with Osaka University, Suita, Japan. In 2017, he was a Visiting Professor with the City University of Hong Kong, China. He is currently a Professor with the Department of Information and Communication System, Hohai University, Changzhou, China, and a Distinguished Professor with the Dalian University of Technology, Dalian, China. He has the authored over 300 papers published in related international conference proceedings and journals, including the IEEE COMST, IEEE TII, IEEE TMC, IEEE TVT, IEEE TIE, IEEE TPDS, IEEE TETC, IEEE IoT journal, IEEE TETCI, IEEE TCC, IEEE Systems journal, the IEEE Sensors journal, the IEEE Wireless Communications, the *IEEE Communications Magazine*, and the *IEEE Network Magazine*. He holds 120 patents. His current H-index is 30 and i10-index is 77 in Google Citation (Google Scholar). The total number of citation of his papers by other people is over 3884 times. His current research interests include the Internet of Things, industrial Internet, mobile computing, artificial intelligence, and security.

Dr. Han received the ComManTel 2014, ComComAP 2014, Chinacom 2014, and Qshine 2016 Best Paper Awards. He has served as the co-chair for over 50 international conferences/workshops and as a Technical Program Committee Member for over 150 conferences. He has served on the Editorial Boards of 16 international journals, including the IEEE JSAC, *IEEE Network Magazine*, the IEEE Systems Journal, the IEEE Access, IEEE/CCA JAS, and *Telecommunication Systems*. He was a Guest Editor of a number of special issues in the IEEE journals and magazines, including the *IEEE Communications*, *IEEE Wireless Communications*, the IEEE Transactions on Industrial Informatics, and *Computer Networks*. He has served as a reviewer for over 60 journals.

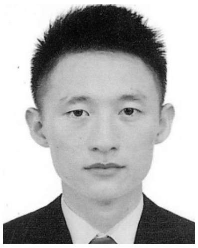

JINGPENG LIANG was born in Fuyang, Anhui, China, in 1993. He received the bachelor's degree in communication and information system from Sanjiang University, Nanjing, China, in 2017. He is currently pursuing the master's degree with the Institute of IOT Engineering, Jiangnan University, Wuxi, Jiangsu. His current research interests include the wireless propagation and wireless channel modeling.

RONG DAI was born in Taizhou, Jiangsu, China, in 1995. She received the bachelor's degree from the Tongda College, Nanjing University of Posts and Telecommunications, in 2014. She is currently pursuing the master's degree with the Institute of IOT Engineering, Jiangnan University, Wuxi, Jiangsu. Her current research interests include wireless propagation and wireless channel modeling.

ZHENG-QUAN LI (M'15) was born in Enshi City, Hubei, China, in 1976. He received the B.S. degree from the Jilin University of Technology, in 1998, the M.S. degree from the University of Shanghai for Science and Technology, in 2000, and the Ph.D. degree from Shanghai Jiaotong University, in 2003. From 2004 to 2010, he was an Associate Professor with Yangzhou University, Yangzhou, China. From 2010 to 2016, he was a Professor with China Jiliang University, Hangzhou, China. He is currently a Professor with the Jiangsu Provincial Engineering Laboratory of Pattern Recognition and Computational Intelligence, Jiangnan University, Wuxi, China. Since 2008, he has been a Post-Doctoral Researcher with the Department of Information Science and Engineering, Southeast University, Nanjing, China. His current research interests include wireless channel modeling, channel estimation, and massive MIMO coding.